Investigation on Electromagnetic Performance of Induction Motor with Rotor Bar Faults considering Motor Current Signals

Yu-Seop PARK
Dept. of Electrical Engineering, Korea National University of Transportation, Chungju, Korea
yspark @ut.ac.kr

***Abstract*—This paper deals with electromagnetic torque and current characteristics of an induction motor with rotor bar breakage, and electromagnetic field analysis based on finite element method and motor current signal analysis is performed according to various load conditions. Although various monitoring techniques of rotor bar breakages were dealt with in previous studies using MCSA, they cannot be, in fact, applied to every case. Therefore, in this paper, electromagnetic field analysis of induction motor with various rotor bar fault conditions is performed to establish fault monitoring criteria in MCSA method. This study employs 0.4(kW) squirrel cage induction motor, and experimentally measured torque and current supports the analysis results.**

***Index Terms*—current, fault, induction motor, torque, rotor.**

I. INTRODUCTION

Electrical machines are essential elements for various industrial applications, so the interests on their relevant fault diagnosis have become very high. Therefore, the studies on fault detection for various electrical machine systems have been performed, such as DC machines [1], induction machines [2]-[7], permanent magnet synchronous machines [8]-[14], and sensors [15]-[17]. Among various types of machines, due to its strong durability, easy maintenance and low manufacturing cost, induction motors have been widely applied to various industrial parts featuring 80(%) of the motors in use [18]. However, the faults by their general hostile operating condition can result in huge financial losses to industrial area. From the previous researches, the fault types of induction motors can be divided into 4 parts, such as mechanical faults including broken bearings, stator faults including inter-turn shorts, and rotor faults including broken rotor bars [19]. Among various fault types, in fact, the ratio of rotor bar fault occurrence is not relatively high. However, the rotor faults can generate distorted air-gap flux density, and it is directly related to torque ripple causing noise and vibration. Therefore, this fault type cannot be ignored, and it should be monitored and detected with other faults in induction motors. So far, plenty of researches have been performed with introducing new techniques. In particular, motor current signal analysis (MCSA) method offers high reliability to monitor the rotor faults [20]-[25]. In those studies, a broken rotor bar was detected by monitoring side band frequency, which can be calculated by the function of both slip and source frequency. Besides, previous related studies confirm that the failure of non-consecutive bars is fairly common in large cage induction motors, and its analytical research was performed showing the trend of left side band frequency in a double bar breakage as a function of the relative position of the bars [25]. However, since the characteristics of induction motors are varied by their speed according to load conditions, the trend presented in previous study are not for every case, and the theory cannot be applied if the slip is varied. For this case, since their fault characteristics are not presented, wrong fault determination can be possible. Therefore, this paper deals with the influence on current characteristics of squirrel cage induction motor with non-consecutive bar breakage according to load condition based on electromagnetic field characteristic analysis to establish more accurate fault monitoring criteria with MCSA. For this study, in Chapter II, fault characteristics with one rotor bar fault are addressed to determine effective slip condition for diagnosis. On the other hand, in Chapter III, a solution is proposed for non-consecutive rotor faults with experimental verification. Finally, in Chapter IV, a conclusion is made to improve conventional MCSA method.

This was supported by Korea National University of Transportation in 2020.

II. ELECTROMAGNETIC CHARACTERISTICS OF SQUIRREL CAGE INDUCTION MOTOR WITH ONE BROKEN ROTOR BAR

The rated specification of the analysis model is presented in Table I, and its rated slip s is 0.05 as indicated in the table. The slip s is calculated by $s=(N_s-N_m)/N_s$. Here, N_s and N_m are respectively synchronous speed and mechanical rotating speed. In this paper, the synchronous speed is 1,800(rpm). When the rotor bar of induction motor is broken as shown in Fig. 1, or when the conductivity of the rotor bar is deteriorated, the electromagnetic force is varied and this phenomenon is related to the current value flowing the rotor bars. The induction motor can be simplified as equivalent circuit as shown in Fig. 2, and the secondary impedance consisted of resistance and reactance is the function of the slip s. In other words, as the value of slip s closes to 0 (higher speed), the secondary impedance becomes very high resulting in very low current value to generate electromagnetic torque. Even when the broken rotor bar is emerged as shown in both Fig. 1 c) and in Fig. 2 c), since its

TABLE I. RATED SPECIFICATION OF ANALYSIS MODEL

Specification	Value	Specification	Value
Voltage	220(V)	Current	2.2(A)
Frequency	60(Hz)	Speed	1710(rpm)
Output Power	0.4(kW)	Efficiency	75(%)
Pole Numbers	4	Rated Slip	0.05

Digital Object Identifier 10.4316/AECE.2020.04005

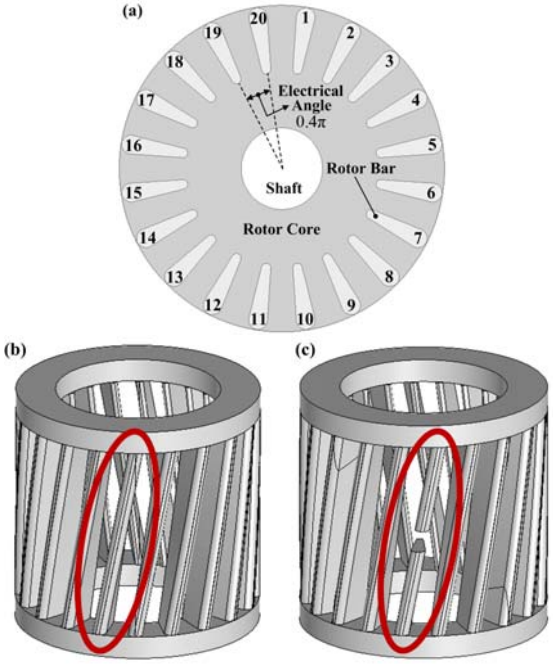

Figure 1. Rotor bar in Squirrel Cage Induction motor: (a) analysis model, (b) healthy rotor, (c) faulty rotor

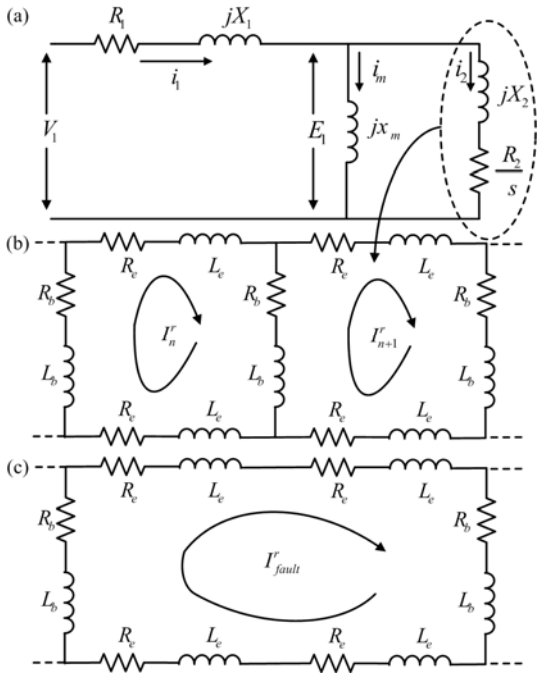

Figure 2. Machine parameters: (a) equivalent circuit, (b) healthy rotor, (c) faulty rotor.

impedance is already high, the current value is not highly varied. However, in large slip condition, the fault resulting dramatic current reduction with high impedance of rotor side, so the electromagnetic torque is deteriorated.

In this paper, to confirm the effects of the conductivity variation in an aluminum rotor bar on the torque characteristics, related electromagnetic field analysis is firstly performed. In the analysis, input condition including voltage and frequency is identical, and the conductivity of an aluminum rotor bar is only varied.

Fig. 3 shows the torque characteristics obtained from electromagnetic field analysis according to slip conditions and the conductivity of an aluminum rotor bar. Here, the conductivity of healthy rotor bar is 38,000,000 (siemens/m),

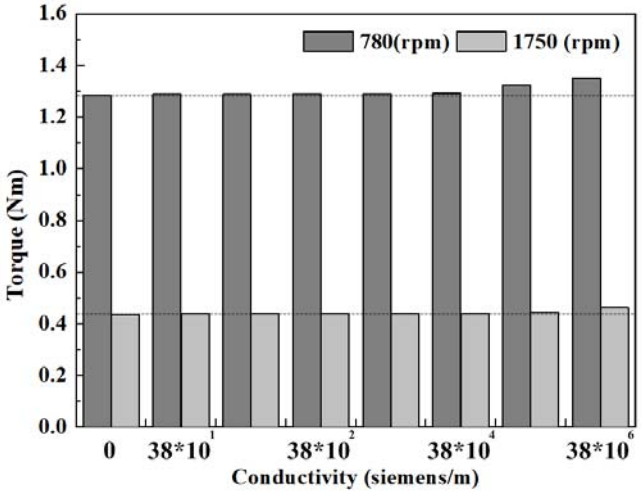

Figure 3. Torque characteristics obtained by electromagnetic field analysis according to the slip conditions and the conductivity of aluminum rotor bar.

and the conductivity 0 (siemens/m) is equal to a broken rotor bar. As can be confirmed from the figure, the value of torque is deteriorated according to the aluminum conductivity. From the figure, flowing two facts are confirmed. At first, the torque of induction motor is reduced by a broken rotor bar when the conductivity of aluminum is deteriorated. In the second place, the torque reduction can be visibly found in higher slip condition, namely low speed condition, while it is hard to find the difference between healthy bar and broken rotor bar in lower slip condition, namely in high speed condition of induction motor.

Fig. 4 shows the more specific torque characteristic analysis results according to slip conditions to present the specific value of slip condition to confirm torque reduction by the broken rotor bar. In this figure, it can be reconfirmed that the torque reduction is found in higher slip condition. Besides, the limited value of the slip can be determined as about 0.2 to monitor visible torque difference. As visible torque reductions are found over 0.2 slip conditions, the increased phase current are presented in similar conditions. At this point, the limited slip condition to present fault characteristic caused by a broken rotor can be determined as 0.2 slip condition. As mentioned above, the rated slip condition of the analysis model is 0.05, so it can be noticed that the fault characteristics, such as reduced torque and increased current, are cannot be easily detected during its normal operation. For the experimental verification of the torque deterioration mentioned above, this paper constructed

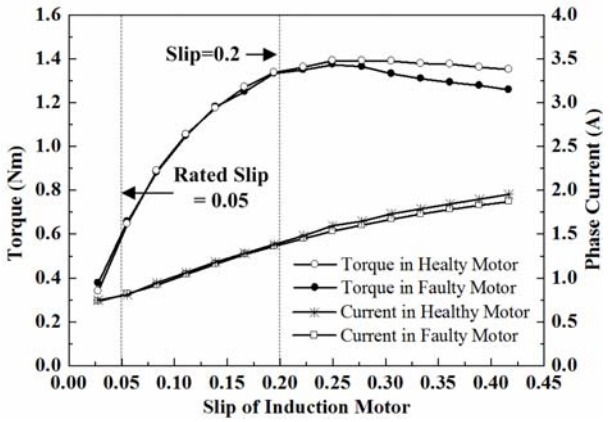

Figure 4. Torque characteristics obtained by electromagnetic field analysis according to the slip conditions and the existence of broken rotor bar.

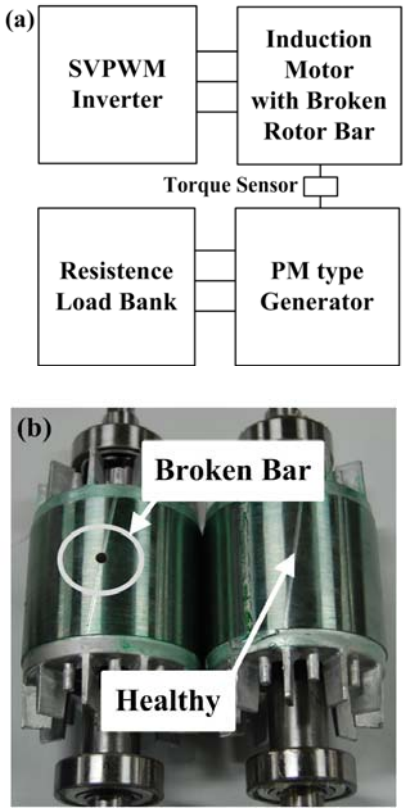

Figure 5. Experimental set construction: (a) experimental set description, (b) rotor with broken rotor bar.

experimental set as presented in Fig. 5 a) and the artificial broken rotor bar in Fig. 5 b). In this experimental set, the torque sensor is located between induction motor and permanent magnet (PM) type generator connected to resistance load for slip variation. To confirm the effect of a broken rotor bar on motor characteristics, the experiment in no-load condition is firstly performed, and Fig. 6 compares

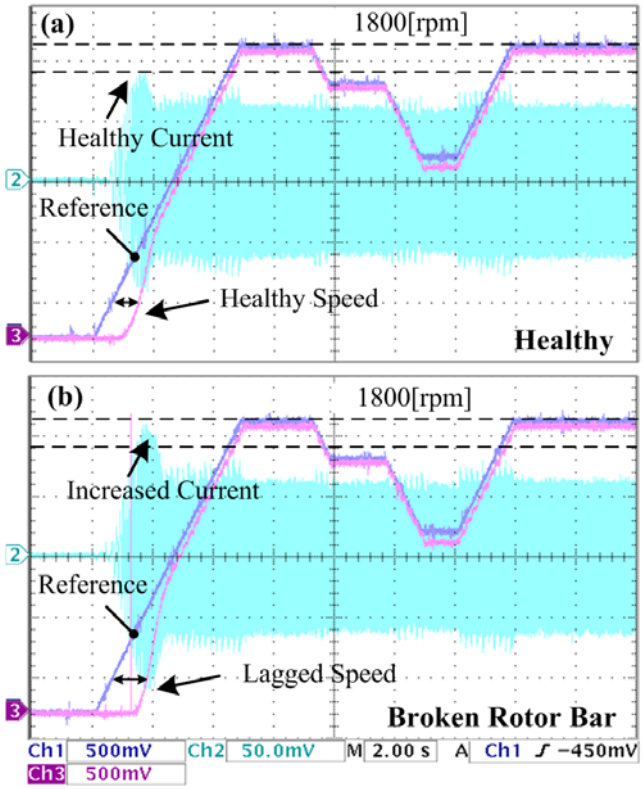

Figure 6. Experimental speed and phase current characteristic in no-load condition: (a) healthy rotor, (b) faulty rotor.

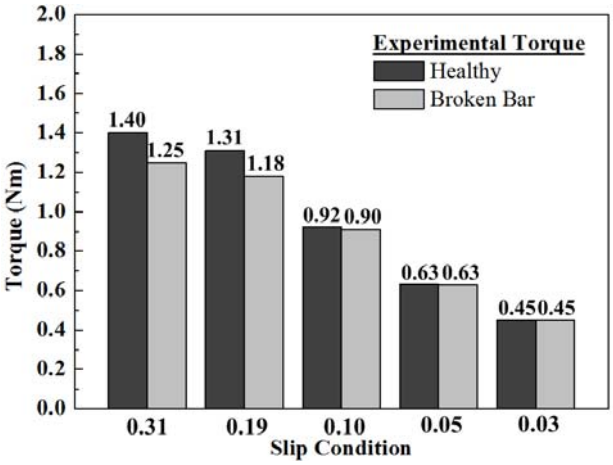

Figure 7. Experimental torque characteristic comparison with various slip conditions according to a broken rotor bar existence.

the speed and current characteristics according to the fault existence. Here, as the speed of the induction motor closes to synchronous speed 1800(rpm), the slip closes to zero. In the figure, it can be confirmed that the speed and current characteristic in high speed (low slip condition) have non-visible difference. On the other hand, when the induction motor with broken rotor bar starts operating (high slip condition), the lagged speed characteristic and increased phase current characteristics are found. Therefore, it can be also confirmed that the speed characteristics in low slip condition are not highly affected by the broken rotor bar. Besides, Fig. 7 compares the torque characteristics in various slip conditions. As presented before, the fault characteristics are not visibly found in low slip conditions while decreased values are measured. In particular, as presented in electromagnetic field analysis mentioned above, we can find that the visible torque difference between healthy motor and faulty motor is emerged over 0.2 slip condition. Therefore, the electromagnetic field analysis performed in this paper can be validated.

So far, with various techniques, the monitoring technology of broken rotor bar has been actively developed, and it is well known that motor current signal analysis (MCSA) offers high reliability to monitor the fault. In MCSA method, the sideband frequency f_b is calculated by (1). Here, s is the slip of induction motor, and f_o indicates supplied current fundamental frequency.

$$f_b = (1 \pm 2s) f_o \tag{1}$$

The entire experimental set for induction motor current signal analysis according to slip is constructed as shown in Fig. 8, and the parameters to obtained sideband frequency in

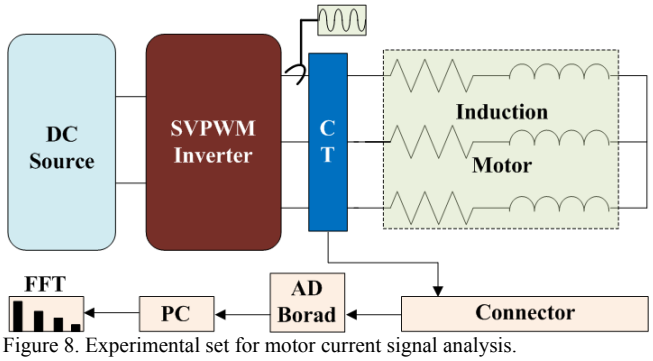

Figure 8. Experimental set for motor current signal analysis.

TABLE II. Parameters to Obtain Sideband Frequency

Specification	Value	Specification	Value
f_o	60(Hz)	N_s	1,800(rpm)
s	0.05	N_m	1,710(rpm)
Upper side f_b	66	Lower side f_b	54

rated speed are presented in Table II as reported in previous study [25].

In Fig. 9, the motor current signals are presented according to the fault existence. This experiment results are obtained in no-load condition, and it can be noticed that the side band frequency mentioned in previous studies is not emerged. Since, in this no-load condition, the slip is very close to zero, the current value flowing aluminum rotor bar is very low. As mentioned before, we confirmed that the fault characteristics, such as torque and phase current, could not be easily found in this slip condition. This can be also applied to MCSA. In other words, the side band frequency caused by a broken rotor bar cannot be easily found in the low slip conditions, and over 0.2 slip conditions are required to apply MCSA. This can be verified by the experimental results, and Fig.10 presets the detected side band frequency caused by a broken rotor bar according to various slip conditions.

As mentioned before, the sideband frequency becomes visible as the value of slip condition is increased. In particular, in rated speed (slip=0.05), the side band frequency is hard to detect, and the right side component is not detected. On the other hand, in slip 0.19 condition, the detected side band frequency is very visible, and right side component is also detected as well. In this point, very important conclusion can be made. Namely, when the induction motor is operated in rated speed, the faults characteristics, such as torque and phase current, have no visible differences, and even the side band frequency cannot be easily detected. Therefore, one can be confused that the operating induction motor has no problem in rotor side, it may cause other related severe faults in induction motor system. Besides, to apply MCSA for the detection of a broken rotor bar, the special experimental set is required to

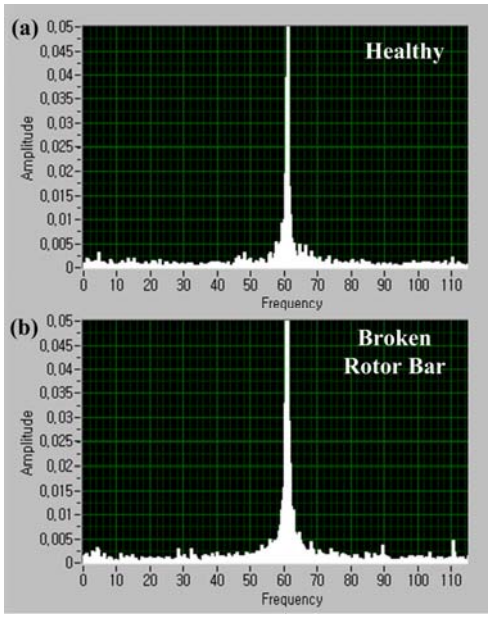

Figure 9. Motor current signal according to fault existence in no-load condition.

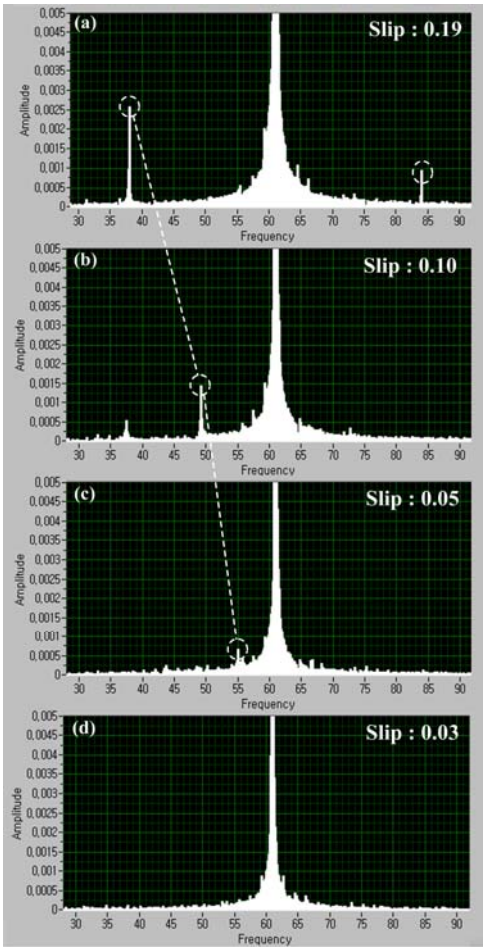

Figure 10. Detected sideband frequency caused by a broken rotor bar according to slip conditions: (a) slip=0.19, (b) slip=0.1, (c) slip=0.05, (d) slip=0.03.

adjust slip conditions, and monitoring the side band frequency in over 0.2 slip conditions should be performed regularly.

III. Investigation on Electromagnetic Performance with Two Non-consecutive Broken Rotor Bars

The detailed rotor bar arrangement dealt with in this paper was presented in Fig. 1. In particular, the rotor of the analysis model has 20 slots with 20 aluminum rotor bars as presented in the figure. As mentioned before. the electromagnetic field characteristic analysis performed in this paper considers the conductivity of the aluminum rotor bars as zero when they are broken, and torque characteristics and current characteristics are analyzed according to the distance of each bar. As indicated in the figure, the electrical distance between consecutive bars is 0.4 π in radian and the analysis is performed according to the non-consecutive rotor bar breakages. In a previous study, the consideration of non-consecutive rotor bar breakages in MCSA was dealt with [25]. This research mentioned that the ratio between the amplitude of the left sideband harmonics in the cases of double and single bar breakage coincides with the ratio between the amplitudes of the *pth* inverse flux density components of the fault field. Besides, from an approximate analysis performed in the previous study, the following expression (2) was presented in the condition that the saturation is neglected. Here, $i_{Ls,double,pu}$ presents the ratio of left side band frequency value in double bar breakages to that in one bar breakage according to the position of broken

rotor bars, and P and α_{bi} are respectively the number of poles and electrical distance in radian of the double broken rotor bars [25].

$$i_{Ls,double,pu} = \left| \frac{I_{Ls,double}}{I_{Ls,simple}} \right| = \left| 2\cos(p\alpha_{bi}) \right| \quad (2)$$

According to this expression, the left side band frequency of induction motors with double rotor bar breakages is expressed as shown in Fig. 11. As shown in the figure, a certain position of two broken rotor bar shows even less value than one broken bar that can result in wrong diagnosis.

In this paper, to confirm whether the conventional theory can be applied to the analysis model according to various slip conditions, fault types were constructed as shown in Fig. 12 and Table III. In the figure, the type A is single broken rotor bar condition, and the type B is consecutive broken rotor bars of 0.4π (No.1-No.2). Furthermore, the type C and the type D are respectively non-consecutive conditions of 0.8π (No.1-No.3) and 1.2π (No.1-No.4).

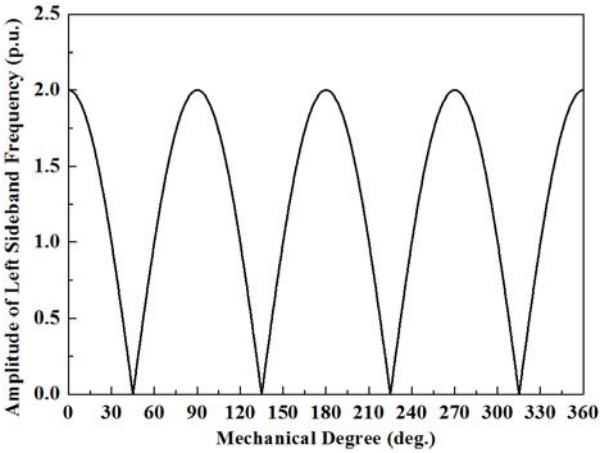

Figure 11. Amplitude of left side band frequency in 4 pole induction motors with double bar breakages according to the distance of broken rotor bars presented in previous study.

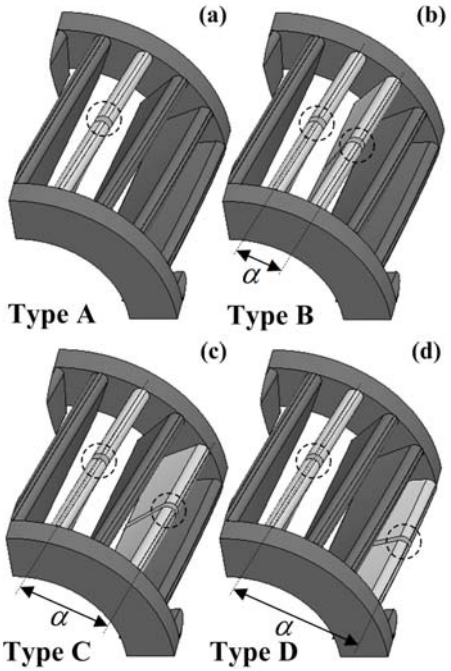

Figure 12. Artificially broken rotor bar in experimental set: (a) single broken rotor bar, (b) consecutive double broken rotor bars(0.4π), (c) nonconsecutive double broken rotor bars(0.8π), (d) nonconsecutive double broken rotor bars(1.2π).

TABLE III. FAULT CONDITIONS FOR ANALYSIS

Fault Condition	Broken Rotor Bar	Electrical Angle	Fault Condition	Broken Rotor Bar	Electrical Angle
1	-	-	12	No.1/No.11	4.0 π
2	No.1	-	13	No.1/No.12	4.4 π
3	No.1/No.2	0.4 π	14	No.1/No.13	4.8 π
4	No.1/No.3	0.8 π	15	No.1/No.14	5.2 π
5	No.1/No.4	1.2 π	16	No.1/No.15	5.6 π
6	No.1/No.5	1.6 π	17	No.1/No.16	6.0 π
7	No.1/No.6	2.0 π	18	No.1/No.17	6.4 π
8	No.1/No.7	2.4 π	19	No.1/No.18	6.8 π
9	No.1/No.8	2.8 π	20	No.1/No.19	7.2 π
10	No.1/No.9	3.2 π	21	No.1/No.20	7.6 π
11	No.1/No.10	3.6 π			

On the other hand, as shown in Fig. 13, in the experimental set, the induction motor is directly connected to permanent magnet (PM) type generator with resistance load bank, so the slip condition of the induction motor can be varied by adjusting the value of load resistance.

At first, the experiment for type A and type B is performed with MCSA to compare the amplitude of left side band frequency. As shown in Table IV, when the rated slip of the analysis model is 0.041, the left side band frequency of type B is approximately 2 times than that of type A as reported in previous study [25]. However, when the slip of the analysis model is varied, the 2 times value of the amplitude is not remained any more, and it is decreased as the slip becomes larger as presented in Table IV. Therefore, since the slip conditions can be varied when the induction

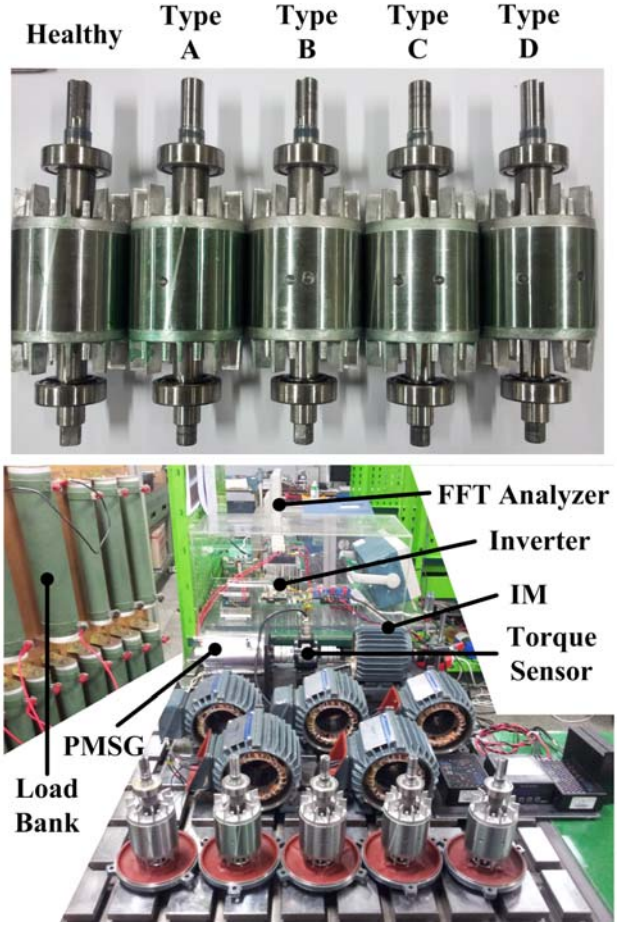

Figure.13. Experimental set with artificially broken rotor bars and PM generator directly connected to induction motor

TABLE IV. EXPERIMENTAL AMPLITUDE OF LEFT SIDE SAND FREQUENCY (P.U.) IN FAULT FYPE B CONDITION ACCORDING TO SLIP VARIATION

Slip s	Value	Slip s	Value	Slip s	Value
0.041	2.30	0.081	1.86	0.166	1.76

motor is employed to other industrial applications, one cannot be assure that the conventional theory can be applied to every case.

In this paper, to provide the fault detection criteria of squirrel cage induction motors, the electromagnetic field analysis according to various fault conditions is performed by finite element method, which is widely applied for the characteristic analysis of electrical machines with high reliability. The fault conditions for the analysis are presented in Table III. Here, fault condition 1 is the healthy motor, and fault condition 2 is the single broken rotor bar. In addition, from fault condition 3 to 21, the non-consecutive broken rotor bar conditions are expressed by rotor bar numbers and electrical angle between the double broken rotor bars as indicated in Fig. 12. Since the number of poles in the analysis model is 4, and the number of slots in rotor is 20, the 5 slots occupy 1 pole.

Above all, Fig. 14 shows the torque characteristics obtained by electromagnetic field characteristic analysis according to slip and fault conditions. As easily anticipated, the torque is deteriorated by the broken rotor bar, and condition 3, which is the consecutive rotor bar breakage, shows mostly deteriorated torque characteristics. In the second place, very important fact can be found in another torque characteristic according to fault conditions presented in Fig. 15. As can be confirmed in the figure, the trend of torque variation follows the conventional theory shown in Fig. 11 at 1300(rpm), namely low slip conditions. However, as the slip is increased, the torque difference becomes very small. In particular, in 600 (rpm) condition, it is very hard to find the difference except for consecutive rotor bar breakage condition 3 and 21. In this point, it can be confirmed that the varying ratio is different according to slip conditions, and Fig. 16 presents the double value of the ratio of maximum torque to minimum torque and its curve fitted data according to slip conditions. Compared to the experimental results presented in Table IV, it can be noticed that the amplitude of left side band frequency is approximately corresponded to the curve fitted data. Therefore, based on the conventional

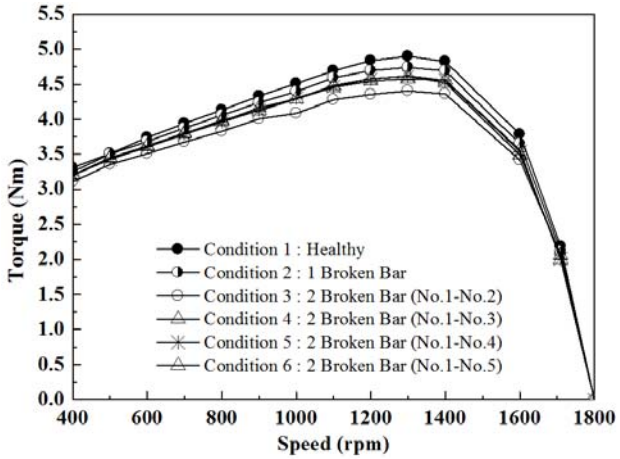

Figure 14. Torque characteristics according to slip conditions.

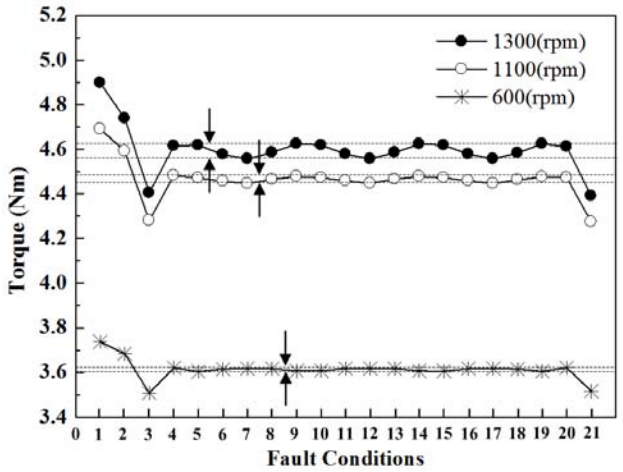

Figure 15. Torque characteristics according to fault conditions.

theory and the curve fitted data, the amplitude of left side band frequency caused by double broken rotor must be modified as shown in Fig. 17. For the verification of the modified trend of left side band frequency according to slip conditions, the experiment is performed. In Fig. 18 to Fig. 21, the left band side frequency according to fault conditions and slip conditions is shown, and they are well corresponded to the modified results. In addition, from the comparison of the left side band frequency amplitude presented in Fig. 22, it can be confirmed that the trend of left side band frequency expressed by (2) does not well fit on various slip conditions.

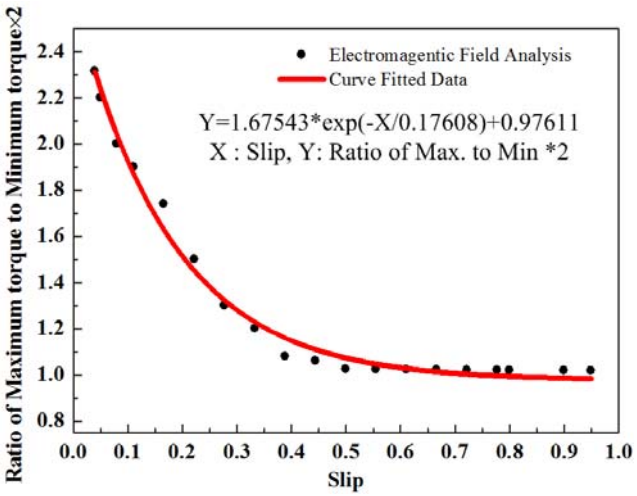

Figure 16. Curve fitted data of ratio of maximum torque to minimum torque according to slip conditions.

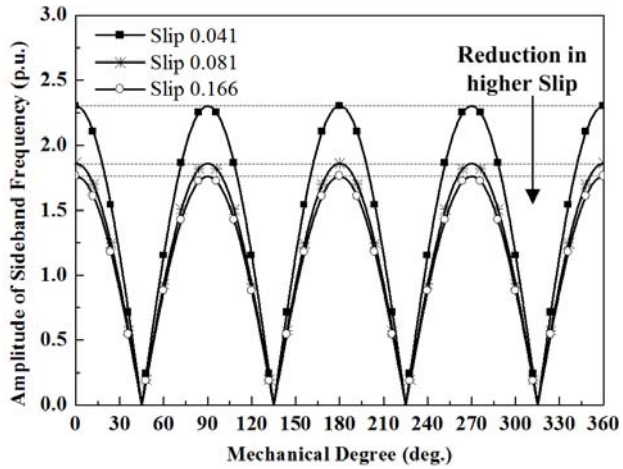

Figure 17. Modified left side band frequency based on curve fitted data.

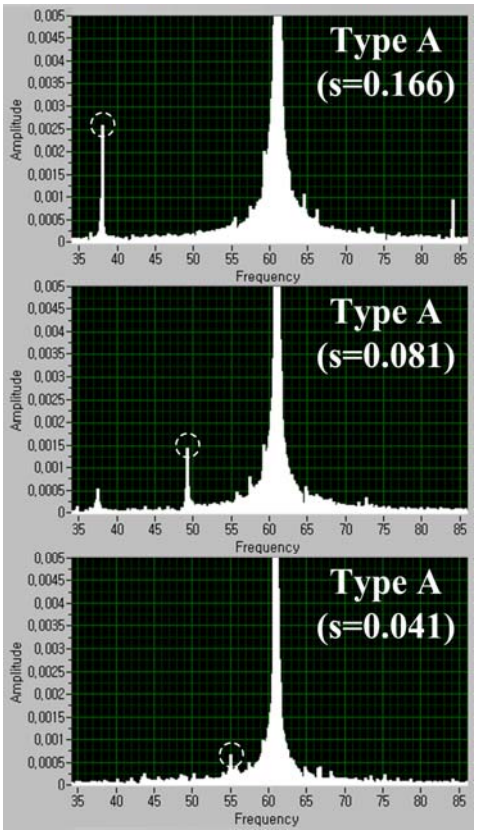

Figure 18. Left side band frequency of Type A according to slip conditions and slip conditions in source frequency 60(Hz).

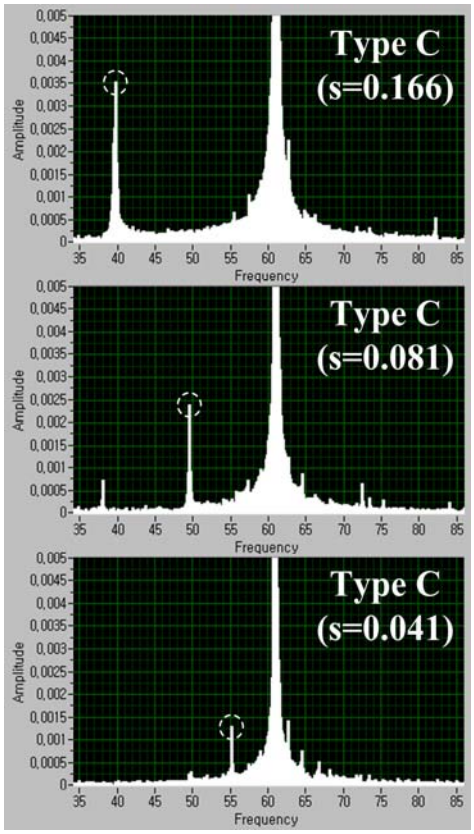

Figure 20. Left side band frequency of Type C according to slip conditions and slip conditions in source frequency 60(Hz).

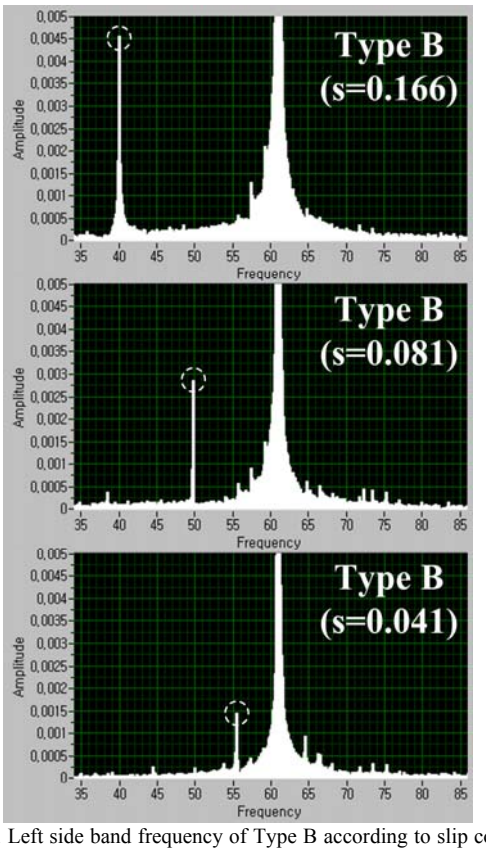

Figure 19. Left side band frequency of Type B according to slip conditions and slip conditions in source frequency 60(Hz).

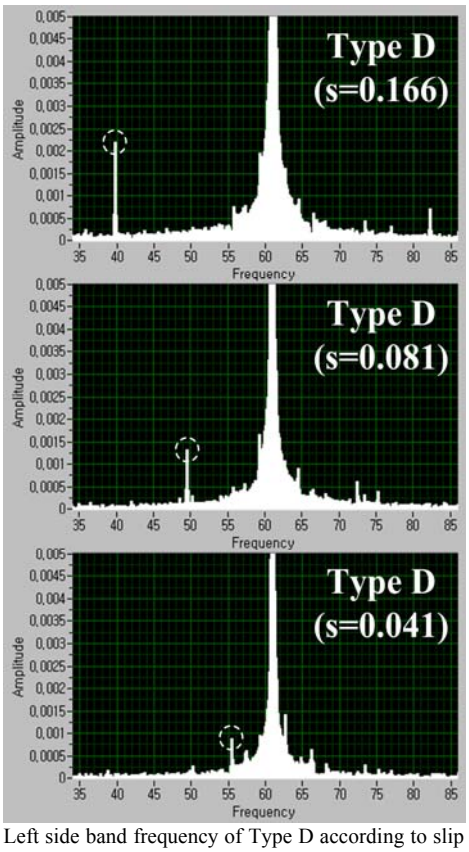

Figure 21. Left side band frequency of Type D according to slip conditions and slip conditions in source frequency 60(Hz).

Finally, based on the analysis and experiment, following 7 steps can be employed for fault monitoring of induction motors which are *Step 1* : modeling of fault rotors based on FEM, *Step 2* : electromagnetic field characteristic analysis according to fault and load conditions, *Step 3* : torque curve derivation, *Step 4*: fault ratio estimation by curve fitting for MCSA method, *Step 5:* experimental set construction with SVPWM inverter and load machine, *Step 6*: side band frequency comparison with applied ratio from FEM, *Step 7*: rotor fault condition diagnosis.

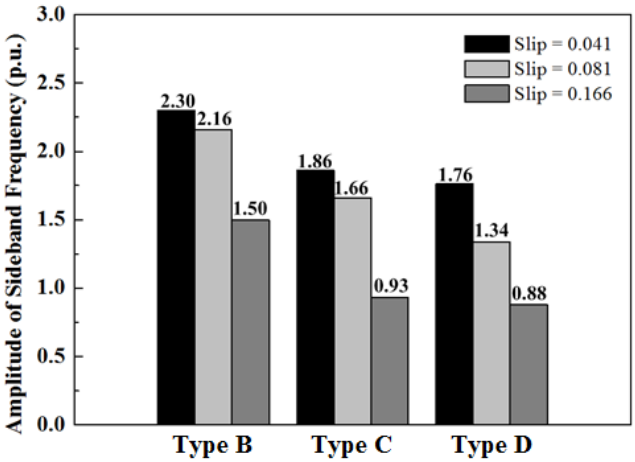

Figure 22. Comparison of experimental left side band frequency.

IV. Conclusion

In this paper, based on electromagnetic field characteristic analysis, the influence on squirrel cage induction motor with various broken rotor bars according to slip conditions are dealt with mostly focusing on electromagnetic torque and current characteristics. Since the reported trend of left side band frequency amplitude has limit for the application to various load conditions with slip variation, this paper presented its modified method using the curve fitted data of torque characteristic analysis results. Since many of induction motors are operated in various slip conditions, the wrong fault determination by MCSA can be possible. On the other hand, the proposed method based on the presented 7 steps for fault monitoring of induction motors can effectively improve the conventional MCSA with consideration of load conditions, so it will contribute to its related industrial applications with high accuracy.

References

[1] S. Postalcioglu Ozgen, "Graphical user interface aided online fault diagnosis of electric motor - DC motor case study," Advances in Electrical and Computer Engineering, vol.9, no.3, pp.12-17, 2009, doi:10.4316/AECE.2009.03003

[2] D. Reljic, D. Jerkan, D. Marcetic, D. Oros, "Broken bar fault detection in im operating under no-load condition," Advances in Electrical and Computer Engineering, vol.16, no.4, pp.63-70, 2016, doi:10.4316/AECE.2016.04010

[3] D. Matic, Z. Kanovic, "Vibration based broken bar detection in induction machine for low load conditions," Advances in Electrical and Computer Engineering, vol.17, no.1, pp.49-54, 2017, doi:10.4316/AECE.2017.01007

[4] L. Mihet-popa, "Current signature analysis as diagnosis media for incipient fault detection," Advances in Electrical and Computer Engineering, vol.7, no.2, pp.11-15, 2007, doi:10.4316/AECE.2007.02003

[5] A. Metatla, S. Benzahioul, T. Bahi, D. Lefebvre, "On line current monitoring and application of a residual method for eccentricity fault detection," Advances in Electrical and Computer Engineering, vol. 11, no. 1, pp. 69-72, Feb. 2011. doi:10.4316/AECE.2011.01011

[6] A. Simion, "Study of the induction machine unsymmetrical condition using in total fluxes equations," Advances in Electrical and Computer Engineering, vol. 10, no. 1, pp. 34-41, Feb. 2010. doi:10.4316/AECE.2010.01006

[7] M. Drif, A. J. M. Cardoso, "Stator fault diagnostics in squirrel cage three-phase induction motor drives using the instantaneous active and reactive power signature analyses," IEEE Transactions on Industrial Informatics, vol. 10, no. 2, pp. 1348-1360, May 2014. doi:10.1109/TII.2014.2307013

[8] C. P. Salomon, C. Ferreira, G. Lambert-Torres, C. E. Teixeira, L. E. Borges Da Silva, W. C. Santana, E. L. Bonaldi, L. E. L. De Oliveira, "Electrical signature analysis for condition monitoring of permanent magnet synchronous machine," Advances in Electrical and Computer Engineering, vol. 18, no. 4, pp. 91-98, Nov. 2018. doi:10.4316/AECE.2018.04011

[9] H. Saavedra, J.-R. Riba, L. Romeral, "Detection of inter-turn faults in five-phase permanent magnet synchronous motors," Advances in Electrical and Computer Engineering, vol. 14, no. 4, pp. 49-54, Nov. 2014. doi:10.4316/AECE.2014.04008

[10] R. S. Arashloo, M. Salehifar, H. Saavedra, J. L. Romeral Martinez, "Efficiency evaluation of five-phase outer-rotor fault-tolerant BLDC drives under healthy and open-circuit faulty conditions," Advances in Electrical and Computer Engineering, vol. 14, no. 2, pp. 145-152, May 2014. doi:10.4316/AECE.2014.02023

[11] M. Aktas, "A novel method for inverter faults detection and diagnosis in pmsm drives of HEVS based on discrete wavelet transform," Advances in Electrical and Computer Engineering, vol. 12, no. 4, pp. 33-38, Nov. 2012. doi:10.4316/AECE.2012.04005

[12] B.-G. Gu, "Study of IPMSM interturn faults part II: online fault parameter estimation," IEEE Transactions on Power Electronics, vol. 31, no. 10, pp. 7214-7223, Oct. 2016. doi:10.1109/TPEL.2015.2506640

[13] H. Wang, S. Lu, G. Qian, J. Ding, Y. Liu, Q. Wang, "A two-step strategy for online fault detection of high-resistance connection in BLDC motor," IEEE Transactions on Power Electronics, vol. 35, no. 3, pp. 3043-3053, Mar. 2020. doi:10.1109/TPEL.2019.2929102

[14] M. Salehifar, R. S. Arashloo, J. M. Moreno-Equilaz, V. Sala, L. Romeral, "Fault detection and fault tolerant operation of a five phase PM motor drive using adaptive model identification approach," IEEE Journal of Emerging and Selected Topics in Power Electronics, vol. 2, no. 2, pp. 212-223, Jun. 2014. doi:10.1109/JESTPE.2013.2293518

[15] L. Dong, J. Jatskevich, Y. Huang, M. Chapariha, J. Li, "Fault diagnosis and signal reconstruction of hall sensors in brushless permanent magnet motor drives," IEEE Transactions on Energy Conversion, vol. 31, no. 1, pp. 118-131, Mar. 2016. doi:10.1109/TEC.2015.2459072

[16] X. Wang, Z. Wang, Z. Xu ; M. Cheng, W. Wang, Y. Hu, "Comprehensive diagnosis and tolerance strategies for electrical faults and sensor faults in dual three-phase PMSM drives," IEEE Transactions on Power Electronics, vol. 34, no. 7, pp. 6669-6684, Jul. 2019. doi:10.1109/TPEL.2018.2876400

[17] Q. Zhang, M. Feng, "Fast fault diagnosis method for hall sensors in brushless DC motor drives," IEEE Transactions on Power Electronics, vol. 34, no. 3, pp. 2585-2596, Mar. 2019. doi:10.1109/TPEL.2018.2844956

[18] B. Ayhan, M.-Y. Chow, M.-H. Song, "Multiple signature processing-based fault detection schemes for broken rotor bar in induction motors," IEEE Transactions on Energy Conversion, vol. 20, no. 2, pp. 336-343, Jun 2005. doi:10.1109/TEC.2004.842393

[19] J. Faiz, B. M. Ebrahimi, H. A. Toliyat, "Effect of magnetic saturation on static and mixed eccentricity fault diagnosis in induction motor," IEEE Transactions on Magnetics, vol. 45, no. 8, pp. 3137-3144, Aug. 2009. doi:10.1109/TMAG.2009.2016416

[20] Jee-Hoon Jung, Jong-Jae Lee, and Bong-Hwan Kwon, "Online diagnosis of induction motors using MCSA," IEEE Transactions on Industrial Electronics, vol. 53, no. 6, pp. 1842-1852, Dec. 2006. doi:10.1109/TIE.2006.885131

[21] A. Naha, A. K. Samanta , A. Routray, A. K. Deb, "A method for detecting half-broken rotor bar in lightly loaded induction motors using current," IEEE Transactions on Instrumentation and Measurement, vol. 65, no. 7, pp. 1614-1625, Jul. 2016. doi:10.1109/TIM.2016.2540941

[22] A. Bellini, F. Filippetti,G. Franceschini, C. Tassoni, R. Passaglia, M. Saottini, G. Tontini, M. Giovannini, A. Rossi, "On-field experience with online diagnosis of large induction motors cage failures using MCSA," IEEE Transactions on Industry Applications, vol.38, no. 4, pp. 1045–1053, July/Aug. 2002. doi:10.1109/TIA.2002.800591

[23] W. T. Thomas, M. Fenger, "Current signature analysis to detect induction motor faults," IEEE Industry Applications Magazine, vol. 7, no. 4, pp. 26–34, Jul./Aug. 2001. doi:10.1109/2943.930988

[24] M. E. H. Benbouzid, "A review of induction motors signature analysis as a medium for faults detection," IEEE Transactions on Industrial Electronics, vol. 47, no. 5, pp. 984–993, Oct. 2000. doi:10.1109/41.873206

[25] M. R. Guasp, M. F. Cabanas, J. A. A. Daviu, M. P. Sanchez, C. H. R. Garcia, "Influence of nonconsecutive bar breakages in motor current signature analysis for the diagnosis of rotor faults in induction motors," IEEE Transactions on Energy Conversion, vol.25, no.1, pp.80-89, Mar. 2010. doi:10.1109/TEC.2009.2032622